Received: 4 August 2020 | Revised: 8 January 2021 | Accepted: 2 February 2021

DOI: 10.1002/aic.17247

PARTICLE TECHNOLOGY AND FLUIDIZATION

AIChE JOURNAL

# Modeling the breakage stage in spheronization of cylindrical paste extrudates

Liguang Wang[1,2] | Chia Wei Lim[1] | Grace Zhen Li Ng[1] | Sarah L. Rough[1] | D. Ian Wilson[1]

[1]Department of Chemical Engineering and Biotechnology, University of Cambridge, Cambridge, UK

[2]School of Chemical Engineering, The University of Queensland, Brisbane, Queensland, Australia

**Correspondence**
D. Ian Wilson, Department of Chemical Engineering and Biotechnology, University of Cambridge, Philippa Fawcett Drive, Cambridge CB3 0AS, UK.
Email: diw11@cam.ac.uk

**Funding information**
The University of Queensland

## Abstract

Spheronization of cylindrical extrudates on a rotating friction plate involves breakage and rounding. Little attention has been given to the breakage stage and quantitative modeling of this process is scarce. Two simple models are compared with experimental data obtained for the early stages of spheronization of microcrystalline cellulose/water extrudates. Tests were conducted for different times ($t$), rotational speeds ($\omega$), initial loadings, and on pyramidal friction plates with different dimensions. The first model, describing the number of pellets, validated $\omega^3 t$ as a characteristic time scale for the breakage stage. The kinetic parameters obtained by fitting showed a systematic dependence on plate dimensions expressed as a scaled gap width. The second model, a simple population balance, described the evolution of the number and length of pellets. The pseudo rate constants provided insights into the kinetics: extrudates tended to break near the middle, while breakage of smaller pellets was slowed down by more pellet–pellet collisions.

**KEYWORDS**
population balance, pellet size, granulation, microcrystalline cellulose, rate constant

## 1 | INTRODUCTION

Spheronization (also known as marumerization) is a widely used granulation technique in the pharmaceutical sector,[1] which can produce smooth, relatively spherical pellets with a narrow size distribution from a fine powder. It is a two-stage process: in the first stage, the material is mixed with a binder to form a wet mass (a soft solid termed the "dough" or "paste" in different communities) and extruded through a mesh or die plate to generate extrudates of approximately equal diameter.[2] These are then fed into a cylindrical bowl with its axis vertical whose base (the friction plate) rotates at high speed (Figure 1A). The plate motion throws the extrudates against the wall. Collisions with the wall and with other extrudates cause them to break into shorter sections, which travel around the edge of the plate in a "rope" (a toroidal bed: see References 3 and 4), dragged by the protuberances on the plate. The collisions also promote rounding, yielding progressively more spherical pellets[5] (Figure 1C).

Detailed studies of spheronization dynamics, such as References 5 and 6, have shown that breakage and rounding are effectively sequential processes, with the number of pellets changing little after the initial, short, breakage stage. The time taken to obtain pellets of acceptable sphericity is dominated by the later rounding stage, and this has attracted most attention to date, ranging from dimensional analysis[7] and discrete element modeling.[8-10] The literature indicates that the friction plate rotational speed, $\omega$, spheronization time, $t$, and the rheology of the paste are the primary factors governing the rounding process while the amount of extrudates loaded, the friction plate pattern, and extrudate dimensions also play significant roles.

The breakage stage is nevertheless important as it determines the number of pellets and thus their average size, as well as the formation of fines, which may either be retained or lost from the process.[11]

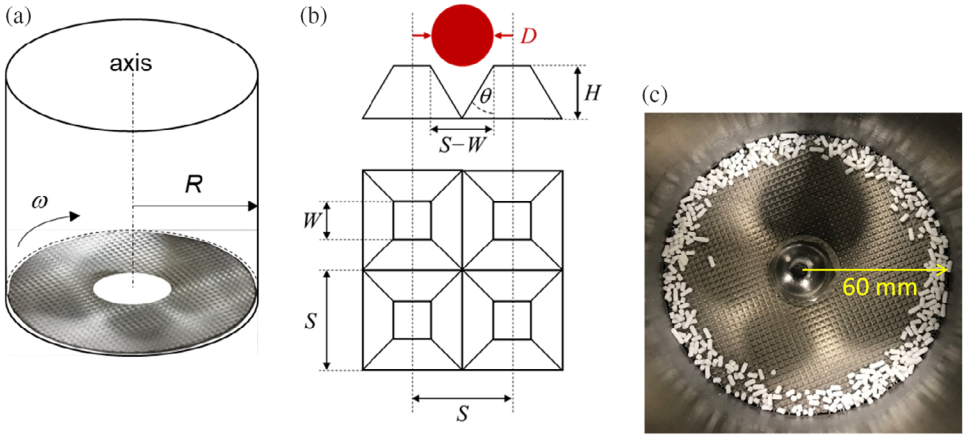


**FIGURE 1** (a) Schematic of spheronizer showing rotating friction plate with square cross-hatched pattern, (b) protuberance pattern of the friction plate, showing key dimensions along with extrudate of diameter *D*, and (c) photograph of plate from above-showing pellets obtained after spheronization of 80 extrudates of diameter 2 mm and length 20 mm (after spheronization with friction plate S2 at 575 rpm for 160 s) [Color figure can be viewed at wileyonlinelibrary.com]

Fines play an important role in rounding as they re-attach to the pellets.[12,13] The tendency to generate fines is governed by the energy involved in collisions (and thus operating conditions), the rheology of the material (and thus formulation), and drying (changing the binder content and hence affecting the rheology, driven by operating conditions such as humidity, temperature, and rotational speed).

Relatively little attention has been given to the breakage stage in spheronization and the authors are not aware of any quantitative modeling of this process. Population balance models are widely applied in other granulation technologies.[14] In these, breakage and agglomeration kernels act in parallel to evolve the pellet number and size distributions: in spheronization, the number distribution is established early and is followed by evolution of *shape*. The current article presents a detailed investigation of breakage kinetics for a simplified spheronization operation, employing the approach reported by Lau et al,[6] where notionally identical experiments are performed in which a set number of extrudates of equal length are spheronized for different times and the pellets analyzed, yielding insight into the kinetics of breakage. The approach was adapted here to improve the amount of data that could be obtained from each test.

The analysis focuses on the yield of pellets from extrudates of given length and the timescale involved. The extrudate diameter is *D*. Wilson and Rough[2] reported that spheronized pellets often have diameters consistent with an initial cylindrical length of 1–1.5*D*. This insight is used here in a simple kinetic scheme describing pellet length, which is compared with experimental results for spheronization using different extrudate loadings and rotational speeds.

A second characteristic length scale in spheronization is that associated with the features on the friction plate. Zhang and coworkers[11,15] investigated the influence of protuberance geometry on spheronization behavior. For the pyramidal cross-hatched patterns employed in this study (see Figure 1B) they identified a critical extrudate diameter, $D_c$, below which cylindrical fragments are expected to sit in the cavities between the protuberances:

$$D_c = \left[\frac{1}{4H^2} + \frac{1}{(S-W)^2}\right]^{-1/2} \quad (1)$$

Giving a scaled extrudate diameter, $D^*$:

$$D^* = \frac{D}{D_c} \quad (2)$$

By conducting experiments with different extrudate diameters, they investigated how the size of extrudates relative to the protuberance geometry affected extrudate attrition and subsequent rounding of pellets. They found that sharp protuberances, quantified by the angle $\theta$ in Figure 1B, gave more fines when $D^* > 1$, which was attributed to a greater amount of attrition as the extrudates moved across the plates rather than sitting in furrows. On the contrary, blunter protuberances (larger $\theta$), similar to those investigated here, gave unimodal pellet size distributions when $D^* > 1$ and bimodal distributions when $D^* < 1$, indicating an effect of $D^*$ on breakage. They did not investigate the effect of protuberance shape on breakage explicitly.

A second, simpler, metric for quantifying the tendency for cylindrical fragments to sit in the cavities between protuberances, considered here, is a dimensionless gap width, $w^*$, defined as.

$$w^* = \frac{S-W}{D} \quad (3)$$

The effect of the rotational speed of the friction plate, $\omega$, on the timescale for extrudate breakage has not been investigated. The time taken for complete spheronization, $t_s$, has been reported to decrease with an increase in $\omega$, and with an increase in the friction plate radius, *R*, so that spheronization tests are often scaled up on the basis of plate rim speed, $R\omega$. Lau et al[6] interpreted this finding in terms of the number of revolutions of the plate and thus number of collisions, which pellets experience. Parkin et al[7] measured pellet velocities in spheronization tests similar to those reported here and found that the rotational speeds were smaller than $R\omega$, but this value provided an upper limit to the range observed. Since the energy in collisions will scale with kinetic energy, and thus $(R\omega)^2$, and the number of collisions is likely to relate to the number of revolutions ($\omega t_s$), Lau et al postulated that the work required to round a pellet would be proportional to $R^2\omega^3 t_s$. This gave $t_s \propto \omega^{-3}$ for a given spheronizer geometry, which was similar to the dependency observed in their experiments, of $t_s \propto \omega^{-3.6}$.

This scaled time of $\omega^3 t$ was also identified in the dimensional analysis of Parkin et al.

One objective of the present work was to determine whether the same time scaling applies to the breakage stage of spheronization. This time scaling is combined with a kinetic scheme to develop a new population balance model for breakage during spheronization. A second objective was to establish the impact of friction plate geometry on breakage behavior. For this short study, $w^*$ (and $D^*$) were manipulated by changing the extrudate diameter and by using friction plates with similar square pyramidal protuberance patterns and different dimensions.

## 2 | MODELING

### 2.1 | Apparent rate of breakage

The number of pellets formed, $N$, after time $t$ was measured and is expressed as the normalized number of pellets, $N^*$,

$$N^* = \frac{N}{N_0} \tag{4}$$

where $N_0$ is the initial number of pellets (i.e., extrudates) loaded into the spheronizer. The experimental data were found to follow the following relationship between $N^*$ and scaled time, $\omega^3 t$:

$$N^* = 1 + \beta\left[1 - \exp\left(-k_N \omega^3 t\right)\right] \tag{5}$$

where $k_N$ is a pseudo rate constant and $\beta$ is a parameter related to the final value of $N^*$. By inspection, $\beta$ can be interpreted as the average number of fragments broken off from each extrudate. Since $\omega^3 t$ (and $R^2\omega^3 t$) captures the effect of process parameters $R$ and $\omega$ on the number of collisions and kinetic energy involved in collisions, $k_N$ can be interpreted as an efficiency, which is expected to be influenced by several factors. In this work, the effect of the spheronizer plate geometry on both terms is considered.

This result can be obtained by modeling breakage as the batch reaction A $\rightarrow (1 + \beta)$B, where species A is an initial extrudate, which breaks once to give (1+ $\beta$) fragments, labeled B, and the rate is first order in A (see Appendix S1). B does not undergo further breakage (but may undergo rounding).

### 2.2 | Rate constants for the sub-processes

A population balance model was developed to understand the kinetics of the extrudate breakage events. The proposed breakage model yielded a set of simultaneous ordinary differential equations (ODEs), which described the number of fragments formed and the lengths of these fragments at a given time. Fitting the model to the experimental data and determining the optimal set of parameters provided insight into the importance of the different kinetic steps.

Wilson and Rough[2] reported that the final diameter of the spherical pellets obtained at the end of the rounding stage is ~1–1.5 times that of the diameter of the cylindrical extrudates fed to the spheronizer. For the extrudates used in these tests, featuring an initial length of 20 mm and diameter 2 mm, each extrudate would be expected eventually to yield ~6 or 7 fragments. The asymptotic value for $N^*$ was found to lie between 5 and 6 under the experimental conditions employed here (see Figure 3).

For modeling purposes, each extrudate was assumed to consist of 6 units of equal length (see Figure 2). Breakage was assumed to occur at one point at any given time and yield two fragments, each having a length of integral multiples of the unit length. Consider the initial extrudate, which comprises 6 units: in one breakage step, it could break into either (i) a 1-unit and a 5-unit fragment; (ii) a 2-unit and a 4-unit fragment; or (iii) two 3-unit fragments. Following the same logic, a 5-unit fragment could break into either a 1-unit and 4-unit fragments, or a 2-unit and a 3-unit fragment, and so on. This discretization scheme is a simplification, and reflects practice in many areas of particle technology whereby size distributions are quantified in terms of size intervals.

Breakage is assumed to be a first-order process in terms of the mother fragment: in effect, collisions with other fragments are not considered to be as important as collisions with the spheronizer wall or the friction plate. Setting $n_i$ to be the number of $i$-unit fragments and scaled time $\tau = \omega^3 t$, the corresponding differential equations are:

$$\frac{dn_6}{d\tau} = -k_{6,1}n_6 - k_{6,2}n_6 - k_{6,3}n_6 \tag{6}$$

$$\frac{dn_5}{d\tau} = -k_{5,1}n_5 - k_{5,2}n_5 + k_{6,1}n_6 \tag{7}$$

$$\frac{dn_4}{d\tau} = -k_{4,1}n_4 - k_{4,2}n_4 + k_{6,2}n_6 + k_{5,1}n_5 \tag{8}$$

$$\frac{dn_3}{d\tau} = -k_{3,1}n_3 + 2k_{6,3}n_6 + k_{5,2}n_5 + k_{4,1}n_4 \tag{9}$$

$$\frac{dn_2}{d\tau} = -k_{2,1}n_2 + k_{6,2}n_6 + k_{5,2}n_5 + 2k_{4,2}n_4 + k_{3,1}n_3 \tag{10}$$

$$\frac{dn_1}{d\tau} = k_{6,1}n_6 + k_{5,1}n_5 + k_{4,1}n_4 + k_{3,1}n_3 + 2k_{2,1}n_2 \tag{11}$$

Solutions were obtained using the fourth order Runge–Kutta method (employing Microsoft Excel user-defined functions) with an integration step size of $0.05 \times 10^7$ s$^{-2}$. This gave good agreement between the analytical and numerical solutions for $n_6$. Identification of the optimal values of the pseudo rate constants was carried out using the Microsoft Excel Solver. The parameter-fitting algorithm minimized the sum of squared residuals between the experimental and predicted values of $n_i$ ($\tau$) for $i$ = 1, 2, ..., 6, in line with the least squares method for the solution of population balance problems.[16] The goodness of fit is quantified using the coefficient of determination, $R^2$, where $R^2$ = 1 – (sum of squares of residuals)/(total sum of squares).

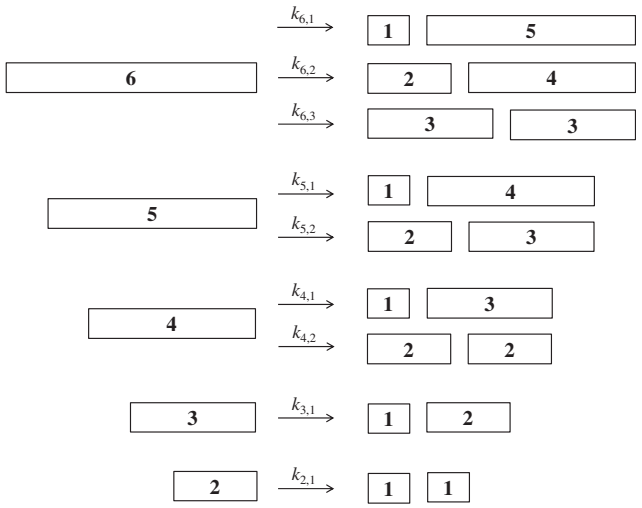


**FIGURE 2** Population balance model. The fragment label indicates the number of "units." $k_{i,j}$ is the pseudo rate constant for each step, with $i$ representing the number of units in the mother fragment and $j$ the number of units in the daughter fragment of shorter length

## 3 | EXPERIMENTS AND METHODS

### 3.1 | Materials

Microcrystalline cellulose (MCC) powder (Avicel® PH-101) was purchased from Sigma Aldrich and used as received. Deionized water was used to prepare the MCC paste.

### 3.2 | Experimental methods

#### 3.2.1 | Preparation of paste

Paste with 47 wt% MCC was prepared in batches of 250 g. A planetary mixer (Kenwood Chef KM200, Kenwood Ltd) was used to mix the MCC powder and deionized water based on the procedure in Reference 11. Briefly, the mixer was run at speed settings "min," 1, 2, 3, and 4 for 1, 2, 3, 3, and 2 min, respectively. Deionized water was added over the first minute. A wooden spatula was used to scrape off any paste stuck to the mixing element or bowl between each mixing step. The prepared paste was then transferred to a polyethylene bag and allowed to rest for at least 2 h in the sealed bag. The paste was used for spheronization on the same day, and unused paste was discarded.

#### 3.2.2 | Compaction and extrusion

Approximately 80 g of paste was loaded into a cylindrical stainless-steel extrusion barrel with a chamber diameter of 25 mm. The paste was compacted by hand for every 10 g of paste loaded to help remove air trapped in the paste. The paste was then compacted to about 1 MPa using a strain frame (Zwick/Roell Z050, Zwick Testing Machines) set up to operate as a ram extruder.[17] The maximum force (i.e., 491 N) was held for 5 s before being released. The compacted paste was subsequently extruded through a concentric single-holed cylindrical die of diameter $D$ and die land length $L$ using a steady ram velocity $v_{ram}$. The extrudate diameter was set by the die land diameter. Table 1 gives the values of $v_{ram}$ and $L$, which produced smooth extrudates without surface fractures while minimizing liquid phase migration.[18] The majority of tests employed a die land with $D$ = 2.0 mm.

**TABLE 1** Extrusion parameters

| | | | |
|---|---|---|---|
| $D$ (mm) | 2.0 | 3.0 | 3.5 |
| $L$ (mm) | 10.0 | 24.0 | 16.0 |
| $v_{ram}$ (mm s$^{-1}$) | 0.55 | 1.25 | 1.70 |

**TABLE 2** Dimensions of friction plates (see Figure 1B)

| | F | S1 | S2 | S3 | S4 |
|---|---|---|---|---|---|
| $W$ (mm) | - | 0.9 | 0.6 | 0.9 | 2.0 |
| $H$ (mm) | 0 | 0.8 | 0.8 | 1.1 | 2.0 |
| $S$ (mm) | - | 2.0 | 2.6 | 3.2 | 6.2 |
| $D_c$ (mm) | - | 0.91 | 1.25 | 1.6 | 2.9 |
| $\theta$ | - | 34.5° | 51.3° | 46.2° | 46.3° |

*Note:* F is a flat plate. Pyramid sharpness (see Figure 1B) $\theta = \tan^{-1}\left(\frac{S-W}{2H}\right)$.

All extrusions were performed at room temperature and humidity. Extrudates were stored in a sealed plastic container immediately after extrusion to prevent water loss.

#### 3.2.3 | Cutting of extrudates

After extrusion, the extrudates were immediately cut into equal lengths of 10$D$ (e.g. 20 mm for 2 mm diameter extrudates) using a scalpel with the aid of graticule stickers, similar to the procedure followed by Bryan et al.[5] The cut extrudates were stored in covered petri dishes to minimize evaporation of water.

#### 3.2.4 | Spheronization

A set number of cut extrudates ($N_0$ = 20 or 80) were loaded into the spheronizer (Caleva Spheronizer 120, Caleva Process Solutions Ltd). Figure 1B shows a schematic diagram of the friction plate, which featured a cross-hatched pattern of square pyramidal protuberances. Table 2 summarizes the dimensions of the stainless steel 316 friction plates employed in this work (photographs provided in Figure S1). The majority of the tests employed a plate with dimensions $W$ = 0.6 mm, $H$ = 0.8 mm, and $S$ = 2.6 mm (labeled in Table 2).

The spheronizer was operated for a set time $t$ at constant rotational speed, $\omega$. The rotational speed was measured using a tachometer. For tests with $N_0$ = 20, the pellets were imaged *in situ* (see below) and the

test continued. Preliminary investigations indicated that these interrupted mode tests gave similar results to continuous ones. For tests with $N_0$ = 80, the pellets had to be transferred to a larger sheet for imaging.

### 3.2.5 | Imaging of pellets and image processing

The pellets generated in the spheronizer were imaged using a digital camera immediately after the friction plate had come to rest. The pellets, which were white in color (see Figure 1C), were placed on a black background to enhance the contrast in the images. A box enclosure was used to block ambient light.

The ImageJ software tool (National Institutes of Health) was used to analyze the images to obtain the number and dimensions of pellets at a given time. The original image was first cropped to remove unwanted outer areas, the distance in pixels for a known length identified, and the number of pixels per unit length was determined using the function "Set Scale" in ImageJ. The image type was changed into 8-bit greyscale, and an optimal threshold was chosen for each image. The "Analyze Particles" function in ImageJ was used to determine the maximum caliper length (i.e., the longest distance between any two points along the outline of the pellet), which was reported as the pellet length.

## 4 | RESULTS AND DISCUSSION

### 4.1 | Scaled run time $\omega^3 t$

Figure 3A shows the evolution of $N^*$ with run time $t$ for different rotational speeds on friction plate S2. For each rotational speed tested, $N^*$ increases with increasing time and approaches a limiting value asymptotically. At a given time, $N^*$ increased with increasing rotational speed. The effect is marked at 11 s, with a factor of five difference in $N^*$ as the rotational speed is increased from 288 to 1150 rpm.

The data are plotted against the scaled run time in Figure 3B. Lau et al[6] found that $\omega^3 t$ was a characteristic time scale for rounding of pellets. Applying this to the data sets here collapse them to a common trend, indicating that this time scaling also holds for the extrudate breakage process (for the range of rotational speeds tested). The figure shows that Equation (5) fitted the comprehensive data set obtained for 575 rpm to Equation (5) well, with $\beta$ = 4.25 and $k_N = 1.88 \times 10^{-7}$ s$^2$. The data sets obtained at other speeds could also be fitted to Equation (5): the values of $\beta$ and $k_N$ were of similar magnitude, ranging from 4.04 to 4.71 and 1.73 to $3.08 \times 10^{-7}$ s$^2$, respectively, with no systematic dependency on $\omega$. It should be noted that collecting data at low values of $\omega^3 t$ (short times for large $\omega$) is challenging as the tests would last 1 s or less. These results indicate that the simple kinetic scheme behind Equation (5) offers a pragmatic basis to analyze breakage data.

### 4.2 | Effect of loading on spheronization

The effect of increasing $N_0$ on extrudate breakage was investigated, and Figure 4 compares the results obtained for $N_0$ = 20 and 80 at 575 rpm. Both data sets fit Equation (5) well, indicating that the same kinetic scheme applies.

Whereas the pseudo rate constants, $k_N$, for the two loadings are similar (both of order $1.9 \times 10^{-7}$ s$^2$), the asymptotic value of $N^*$ (and $\beta$) is smaller for $N_0$ = 80. This indicates that the average final pellet size is larger for the higher loading, suggesting that pellet–pellet interactions retard the later breakage process. This is consistent with the

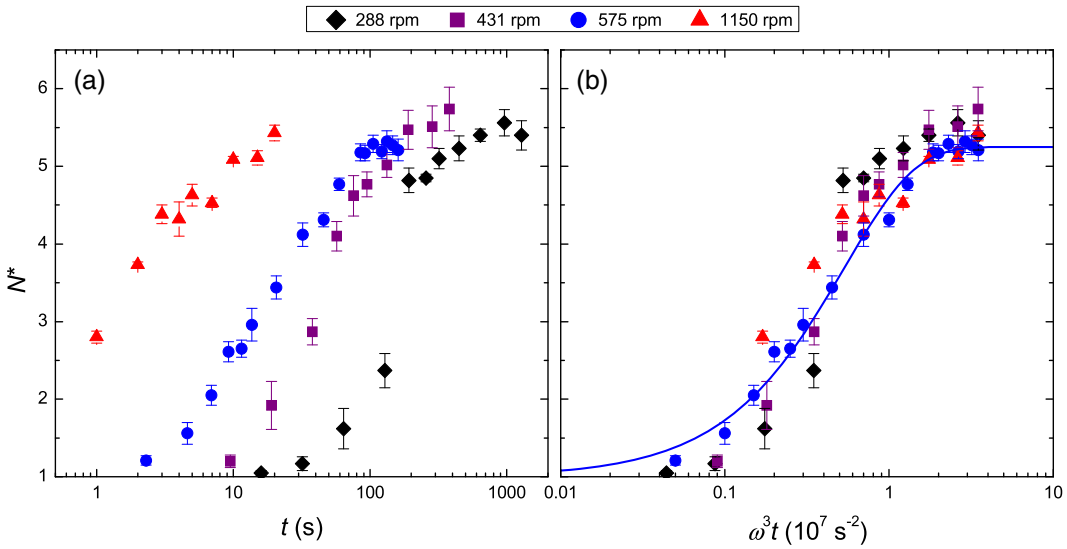


**FIGURE 3** Effect of rotational speed (friction plate S2) on evolution of $N^*$ with (a) run time, $t$, and (b) scaled run time, $\omega^3 t$ (note log axes). Initial load of extrudates, $N_0$ = 20 (with $D$ = 2 mm). The blue line represents the best fit of Equation (5) to the experimental data obtained at 575 rpm: $N^* = 1 + 4.25[1 - \exp(-1.88 \times 10^{-7} \omega^3 t)]$. The color scheme for different values of $\omega$ is employed in subsequent plots. Error bars represent one standard error, obtained from three or five independent runs. The individual data sets are reported in Figure S2 [Color figure can be viewed at wileyonlinelibrary.com]

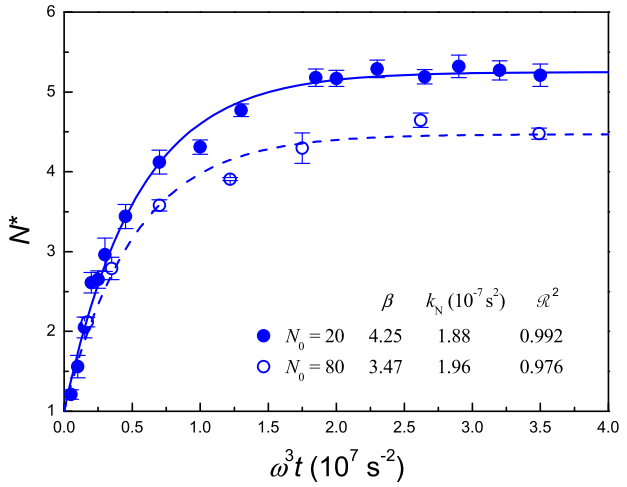


**FIGURE 4** Evolution of $N^*$ with $\omega^3 t$ for different initial extrudate loadings, $N_0$ (with $D$ = 2 mm). The rotational speed (friction plate S2) was 575 rpm. The lines represent the best fit of Equation (5) to the experimental data. Error bars represent one standard error obtained from three or five independent runs [Color figure can be viewed at wileyonlinelibrary.com]

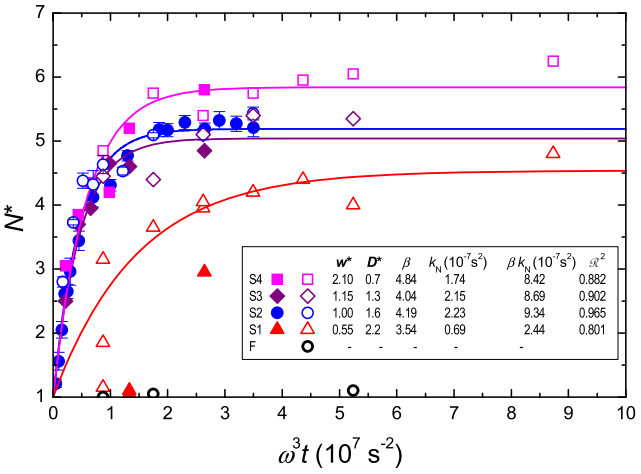


**FIGURE 5** Effect of friction plate dimensions on evolution of pellet number. $D$ = 2 mm, $N_0$ = 20, $\omega$ = 575 (solid symbols) or 1150 rpm (open symbols). Loci show fit to Equation (5), parameters given in Figure 6A [Color figure can be viewed at wileyonlinelibrary.com]

observations of Koester and Thommes,[4] who used particle image velocimetry to visualize pellet movement in the spheronization of extrudates made from a mixture of MCC and α-lactose monohydrate. They found that higher loadings led to lower pellet velocities, which was attributed to higher energy dissipation within the deeper pellet bed.

## 4.3 | Effect of friction plate geometry

A brief study was conducted to quantify the influence of friction plate protuberance dimensions on breakage behavior. Fewer tests were conducted so the data are subject to greater uncertainty. Figure 5 shows the impact of protuberance size on breakage dynamics for the plates in Table 2, with 2 mm diameter extrudates and two plate rotational speeds. Little breakage occurred with the flat plate (labeled F), with the extrudates tending to roll on the plate and bounce off the spheronizer wall. All the plates with pyramidal geometry promoted breakage, with profiles similar in form to those displayed in Figure 3. All the profiles fitted the scaled relationship (Equation (5)), with noticeably slower breakage on plate S1, for which $D^*$ = 2.2 and $w^*$ = 0.55 (see Equation (3)). Extrudates would not be expected to reside or be trapped within the furrows between protuberances in this case.

Figure 6A shows the effect of protuberance dimensions on the breakage model parameters obtained by fitting the data in Figure 5 to Equation (5). The parameter $\beta$ increases with increasing $w^*$, indicating that such geometries promote breakage of 3-unit and 2-unit fragments. The values of $k_N$ are similar for $w^* \geq 1$, and noticeably smaller for $w^* < 1$. Figure 5 also shows that the initial rate of breakage, when expressed in scaled terms, that is, $dN^*/d(\omega^3 t)$, is similar for plates with

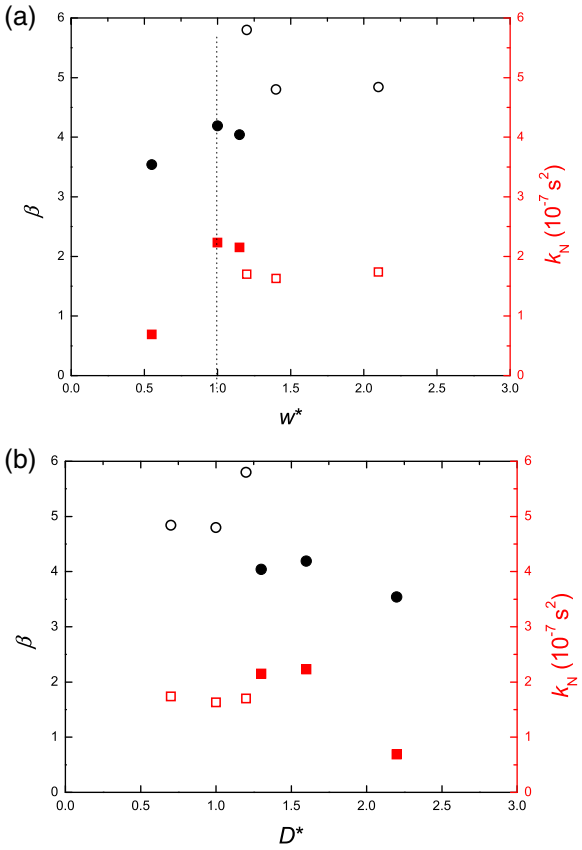


**FIGURE 6** Effect of protuberance geometry, expressed as (a) $w^*$, and (b) $D^*$, on breakage model parameters $\beta$ (circles) and $k_N$ (squares) obtained by fitting data to Equation (5). Solid symbols—$D$ = 2 mm, different plates (Figure 5); open symbols—plate S4, different $D$ [Color figure can be viewed at wileyonlinelibrary.com]

$w^* \geq 1$. Equation (5) indicates that the initial scaled rate is proportional to $\beta k_N$: the values of the product $\beta k_N$ are reported in the figure legend and are similar for $w^* \geq 1$, and lower for $w^* < 1$ (see also

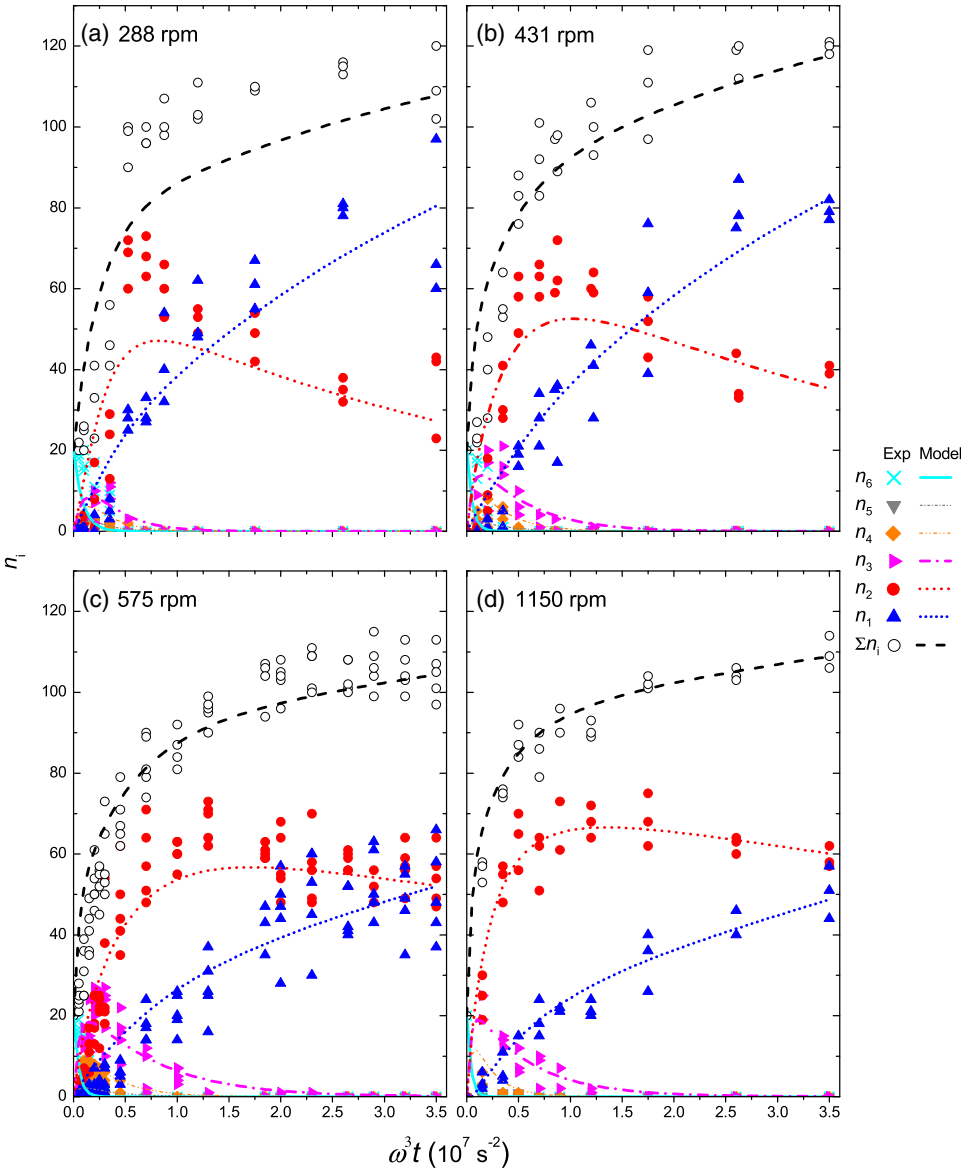


**FIGURE 7** Effect of rotational speed (friction plate S2) on the number of fragments of different length. (a) 288 rpm, (b) 431 rpm, (c) 750 rpm, (d) 1150 rpm. Loci show the fit of the population balance model for $n_1$ to $n_6$, as well as the total number of pellets, with pseudo rate constants presented in Figure 8. Initial extrudate loading, $N_0$ = 20 (with $D$ = 2 mm) [Color figure can be viewed at wileyonlinelibrary.com]

Figure ). This suggests that collisions are less efficient (in terms of breakage) or less energetic in the latter case, where the extrudate will not sit readily in the furrows between protuberances. The kinetic parameter values are also presented in terms of $D^*$ in Figure 6B and show a similar trend, albeit in reverse, owing to their definitions. The scaled gap, $w^*$, offers a more elegant interpretation.

The influence of geometry was also investigated by varying the extrudate diameter from 2 to 3.5 mm with friction plate S4, giving $1.2 \leq w^* \leq 2.1$ and $0.7 \leq D^* \leq 1.2$. Smaller extrudate diameters such as those investigated by Zhang et al[11] were not investigated as they tended to dry out quickly and were therefore not suitable for interrupted experiments due to the time required to prepare extrudates. They also tended to fall through or be caught in the gap between the friction plate and the spheronizer wall. Figure 6 shows similar values of $\beta$ (given the limited number of tests conducted). There is a pattern of $k_N$ values obtained using larger extrudate diameters on plate S4 being higher than those obtained using smaller extrudate diameters on plate S2, even when the $w^*$ values are similar. This is attributed to the difference in strain and stress history experienced by material in preparing extrudates of different diameter. Bryan and Rickenbach[19] measured the yield stress of MCC pastes similar to those studied here, extruded through die lands of different diameters and reported that smaller values of $D$ gave larger yield stresses, while Zhang et al[20] reported different pellet characteristics for pellets obtained from their smallest ($D$ = 1 mm) extrudates. Further careful experiments, in which the rheology of the extrudates is controlled, are required to understand these factors.

The scaled initial breakage rates ($\beta k_N$) for different diameters were similar to those obtained for different plates with $w^* > 1$ (Figure ). Zhang et al[11] investigated the overall spheronization performance of different friction plates and reported that smaller protuberances, associated with $w^* < 1$, favored rounding via more efficient collisions and reducing the tendency of pellets to reside on the friction plate. The two stages of spheronization, therefore, appear to favor friction plate configurations differently: breakage is promoted by extrudates (and pellets) fitting into furrows while rounding is promoted by pellets not residing there.

## 4.4 | Population balance model

Each data point in Figures 3 and 4 represents a time instant where spheronization was halted and the fragments photographed. The number of fragments in each size range at that instant, that is, $n_i(\tau)$, was identified and the data sets for each run fitted to the population balance model.

## 4.5 | Effect of rotational speed

Figure 7 shows the data sets obtained for four different rotational speeds (friction plate S2) for the same initial loading of extrudates ($N_0$ = 20, with $D$ = 2 mm). The profiles are similar to those obtained for a series of chemical reactions in batch mode, e.g. A → B → C, and so forth. The initial extrudates ($n_6$) and long fragments ($n_5$ and $n_4$) break up rapidly and are relatively short-lived, with only 1-unit ($n_1$) and 2-unit ($n_2$) fragments being present in appreciable number after a scaled time of $10^7$ $s^{-2}$. The initial dynamics can be seen in Figure , where the data are presented on log-linear axes.

Figure 7 also shows the fit of the model to the total number of fragments and individual size fractions. The fit of the model is considered satisfactory, given the level of approximation employed, and captures the trends evident in the data. The agreement with individual $n_i(\tau)$ profiles and the total number of fragments, $\sum n_i$, improves with increasing rotational speed. The $R^2$ values for each profile are reported in Table  and show that the agreement is less good at the lower rotational speeds: drying is expected to be more significant under these conditions as the tests last longer.

The $R^2$ values for the $n_5$ and $n_4$ profiles were noticeably lower than those of the other size fractions and were negative in some cases, indicating greater uncertainty in the model in these cases. This is partly a result of the number of these fragments being small and their lifespan short, as mentioned above: the parameter fitting calculation then tends to weight their contribution less strongly. It also means that there is lower confidence in the values of the pseudo rate constants.

The pseudo rate constants obtained for each rotational speed are summarized in Figure 8. Increasing $\omega$ from 287 to 1150 rpm leads to noticeable increases in $k_{6,2}$ and $k_{6,3}$, whereas $k_{6,1}$ and $k_{5,2}$ are almost constant. Both $k_{3,1}$ and $k_{2,1}$ decrease with increasing $\omega$: although small in absolute terms, the trends represent the 3-unit and 2-unit fragments breaking less rapidly than the longer fragments.

For all four rotational speeds tested, the pseudo rate constants for end-breakage for a given $i$-unit fragment, that is, $k_{i,1}$, are smaller than those for mid-breakage, $k_{i,2}$ and $k_{i,3}$. This indicates that breakage occurs preferentially near the middle of each fragment. It should be noted that the values of $k_{5,j}$ and $k_{4,j}$ are subject to large uncertainty, as discussed above. The parameter fitting method generates the most likely set of values, and further experiments, starting with 16.7 and 13.3 mm long extrudates, would be required to determine whether this behavior was followed by these size fractions. Kumar et al[21] reported a similar finding in their studies of an attrition cell with an impeller, in that particles broke most frequently at their center. Detailed imaging of breakage events was not carried out in the current work, but one could expect the largest stresses to be generated at the midpoint of a moving extrudate if one end was pinned in a serration channel and the other end collided with the wall, being analogous to a three-point bending test.[21,22]

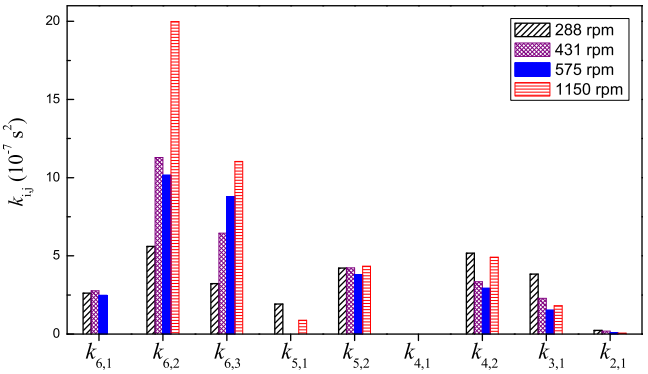


**FIGURE 8** Effect of rotational speed (friction plate S2) on fitted pseudo rate constants $k_{i,j}$. Initial loading of extrudates, $N_0$ = 20 (with $D$ = 2 mm) [Color figure can be viewed at wileyonlinelibrary.com]

The mid-span breakage pseudo rate constants for the initial extrudate, $k_{6,2}$ and $k_{6,3}$ are, in most cases, larger than $k_{5,2}$ and $k_{4,2}$, implying that a longer extrudate has a higher probability of breakage than a shorter extrudate. Both $k_{6,2}$ and $k_{6,3}$ increase with an increase in $\omega$, whereas $k_{5,2}$ and $k_{4,2}$ do not, suggesting that the simple kinetic rate law used here, where only one breakage event occurs per fragment at any given time, does not capture the physics for the 6-unit fragments completely. The effect of extrudate length on breakage behavior is considered further in the next section.

## 4.6 | Effect of loading

Figure 9 shows the experimental data and the fit to the breakage model for the higher initial loading of extrudates ($N_0$ = 80, $D$ = 2 mm) at 575 rpm (friction plate S2), alongside the model results for $N_0$ = 20 at the same rotational speed (Figure 7C). The differences in the fitted curves for $n_2$ to $n_6$ are small, which is consistent with Figure 4, where the pseudo rate constants ($k_N$) for the two loadings are similar. There is, however, a noticeable difference in $n_1$ profiles between the two loadings, with the appearance of 1-unit fragments being slower for the larger loading. The initial dynamics can be seen in Figure , where the data are presented on log-linear axes.

The fit of the model to the data for $N_0$ = 80 is excellent and the $R^2$ value for each profile is reported in Table . The $R^2$ values are all higher than those obtained with $N_0$ = 20, particularly for $n_5$ and $n_4$, indicating greater confidence in the model parameters. The pseudo rate constants obtained for each initial loading are summarized in Figure 10 and show the same pattern, of breakage occurring preferentially at the middle of longer fragments ($k_{6,2}$ and $k_{6,3}$ » $k_{6,1}$; $k_{5,2}$ » $k_{5,1}$; $k_{4,2}$ » $k_{4,1}$). Increasing $N_0$ from 20 to 80 does not affect $k_{6,2}$ and $k_{6,3}$ strongly, but $k_{6,1}$, $k_{3,1}$ and $k_{2,1}$ are all noticeably smaller.

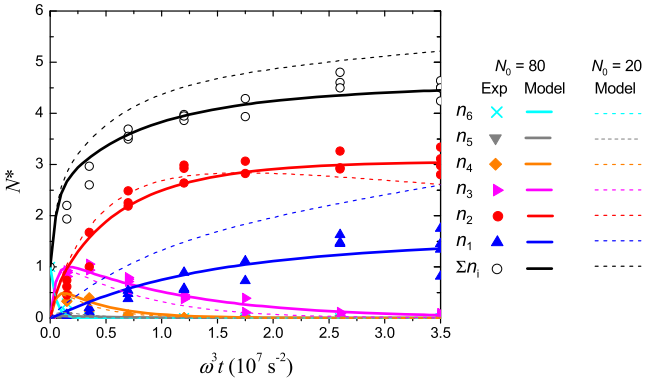


**FIGURE 9** Fit of breakage model to number of fragments for $N_0$ = 80 alongside the modeled profiles for $N_0$ = 20 (Figure 5C, dashed loci). Pseudo rate constants given in Figure 10. Friction plate S2, $\omega$ = 575 rpm, $D$ = 2 mm [Color figure can be viewed at wileyonlinelibrary.com]

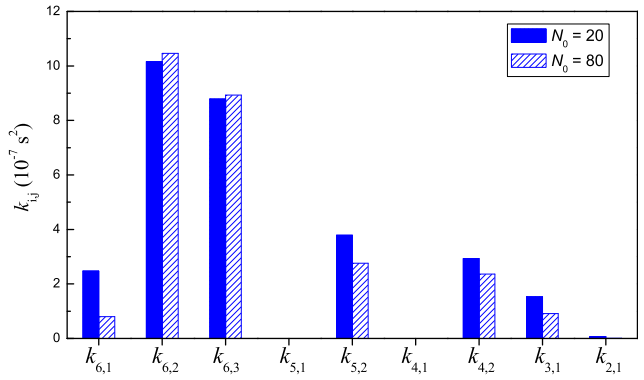


**FIGURE 10** Effect of extrudate loading $N_0$ on pseudo rate constants at rotational speed of 575 rpm (friction plate S2) and $D$ = 2 mm [Color figure can be viewed at wileyonlinelibrary.com]

Comparing the $k_{i,j}$ values in Figure 10 allows the effect of extrudate length to be considered further. The similarity in $k_{6,2}$ and $k_{6,3}$ values is consistent with these steps involving a collision between the initial extrudate and the walls, independent of the number of pellets in the bed: the 6-unit fragments tend to tumble and even become airborne (evident in the videos provided in Reference 7). Smaller fragments tended to accumulate in the rope of material at the friction plate edge (see Figure 1C) and are involved in collisions with other fragments as well as with the wall. The decrease in $k_{5,2}$, $k_{4,2}$, and $k_{3,1}$ values are consistent with lower collision speeds, making it harder to break shorter fragments. This is also consistent with the observation that the larger loading gave a smaller asymptotic value of $N^*$ (and $\beta$, see Figure 4) and larger final pellet size.

Figure 11 shows the effect of pellet length on the likelihood of breakage, represented by ($k_{6,1}$ + $k_{6,2}$ + $k_{6,3}$) for 6-unit extrudates, ($k_{5,1}$ + $k_{5,2}$) for 5-unit pellets, and so forth. Given the uncertainty associated with the $k_{i,j}$ values, some qualitative conclusions can be drawn. The likelihoods for 1-unit and 6-units differ noticeably from the other cases, for both the $N_0$ = 20 and the $N_0$ = 80 results (where the fit to

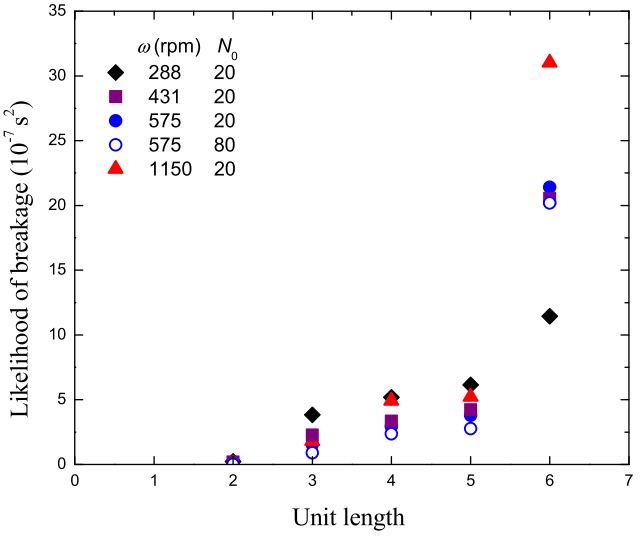


**FIGURE 11** Effect of fragment length on likelihood of breakage, $\sum k_{i,j}$. Solid symbols, $N_0$ = 20 ($k_{i,j}$values in Figure 8); open symbols, $N_0$ = 80 ($k_{i,j}$ values in Figure 10) [Color figure can be viewed at wileyonlinelibrary.com]

the model was more reliable). The high likelihood of breakage for 6-unit extrudates discussed above is evident, while there is a general trend of the likelihood of breakage increasing with length for 3, 4, and 5-unit pellets. An explanation for the latter behavior can be proposed by considering the flexural strength of the pellet material. For a cylindrical rod subject to a force $F$ applied at its center, as in a three-point bending test, the flexural strength $\sigma_f$ is proportional to $FL/D^3$: when this reaches the fracture strength of the material, the rod will break. If the force transmitted in a collision is related to the momentum of the rod, that is, $F \propto \rho L D^2 u_i^2$, where $u_i$ is the rod velocity, then $\sigma_f \propto \rho D \left(\frac{L}{D}\right)^2 u_i^2$ and a lower velocity is required for a longer rod to reach the material's breaking limit. The pellet velocity is, however, likely to be affected by pellet length so this is an incomplete description. Flexural strength considerations can, however, explain the consistently small values obtained for $k_{2,1}$: the flexural strength of short, stubby rods is known to be high (three-point bending tests such as ASTM C1684-13 recommend that the span length to specimen diameter ratio shall be not less than 3) so short pellets are more likely to undergo plastic deformation (and rounding) rather than breaking to give shorter lengths.

There is considerable scope for further investigation of the impact of loading on breakage, as a longer breakage stage will extend the spheronization time via the additional time required to generate shorter fragments. Higher loadings are known to lead to overmassing, which is consistent with many low-speed collisions leading to fusion of fragments rather than breakage.

## 5 | DISCUSSION

Extrudate breakage in spheronization is known to be a random process[2] so it is challenging to predict the evolution of pellet sizes. This

information is needed as this behavior ultimately determines the size distribution of the products. The population balance model presented here proved to be quite effective and provides some insight into the breakage stage of the spheronization process. It gave a good description of both the total number of pellets formed and their length distribution, which gives an approximate indicator of pellet volume. It does not, however, capture the evolution of shape: this is the subject of ongoing work.

The tendency for the initial extrudates and longer pellets to break near their center has been reported in attrition studies but has not, to the authors' knowledge, been reported for spheronization applications. Only one initial extrudate length was considered in this work and there is a need for other lengths to be considered, as industrial operations feature a mixture of extrudate lengths in the initial batch. Extrudates are typically generated by screen and basket devices and the length is often determined by the location of the die hole on the die plate or screen. The effect of extrudate length on $k_{ij}$ values has been determined for one initial length and studies with different lengths would provide insight into dynamics in the rope. If breakage behavior (and thus rounding) could be controlled via extrudate length this would offer a way of improving process reproducibility. Studies of other initial extrudate lengths (e.g., 16.7 and 13.3 mm, representing the $n_5$ and $n_4$ size fractions) would also allow confirmation of the finding that pellets tend to break at the center.

Breakage has been investigated in other applications, particularly comminution, by discrete element method (DEM) simulation (e.g., Delaney et al[23]). In the field of spheronization this technique has been used to investigate the rounding of pellets[8,9] and convective mixing within the rope,[10] for spherical or near-spherical pellets. DEM is well suited to describing the dynamics of extrudates on a rotating friction plate and pellets within a toroidal bed: adding a breakage step to the simulations appears a logical development in the field.

The brief study of friction plate characteristics shows that certain geometric combinations promote breakage. These do not, however, necessarily promote rounding and this offers insights into why investigations of friction plate geometry do not show simple relationships.

Industrial practice is to use higher initial loadings than those investigated here. While the initial step of extrudate breakage was found to be influenced more by interactions between extrudates and the equipment surfaces, pellet-pellet interactions affected the later stages of breakage. It is, therefore, expected that the time for breakage for industrial loading levels will extend beyond those reported here. Since the timescales for breakage and rounding both scale with $\omega^3 t$, the overall dependency on time is expected to scale in a similar manner for different speeds but the dependency on loading remains to be established. Extending the approach used here to such larger loadings will increase the image processing task. Identifying individual pellets for sizing (and shape analysis) can be time-consuming and is well suited to machine-learning approaches, which is the subject of ongoing work.

While the focus on this work has been on breakage as an initial step in spheronization, where it is followed by rounding, it is expected that these results will apply to other operations such as pelletization, where extrudates are broken into shorter lengths but not rounded.

## 6 | CONCLUSIONS

Modeling and experimental studies were conducted to determine the sequence of events involved in the early stages of spheronization of cylindrical extrudates. $\omega^3 t$ has been shown previously to be a characteristic time scale for the overall spheronization process and this work has demonstrated that it also applies to the short, initial, breakage stage. Comparing experimental data using $\omega^3 t$ as the scaled time showed that breakage followed a similar characteristic behavior for the range of rotational speeds tested. The range is representative of those employed in pharmaceutical manufacturing applications, and this result can be utilized as the characteristic time scale when planning experiments and analyzing results.

The evolution of pellet numbers was modeled using two approaches. The first, an overall measure, described the dynamics in terms of an overall gain and a breakage pseudo rate constant. The influence of rotational speed was captured by the $\omega^3 t$ scaling, and the gain was not strongly dependent on the speed. Increasing the initial number of extrudates reduced the gain, which was attributed to more frequent pellet-pellet collisions.

The overall model allowed the impact of friction plate dimensions on breakage to be quantified. The gain and pseudo rate constant were found to be related to the plate dimensions and extrudate diameter in a simple manner when these were expressed as the scaled gap, $w^*$.

The second model, a simple population balance, gave a good description of the evolution of pellet lengths. Extrudates and long pellets were found to break preferentially near their center, while higher loadings reduced the rate of breakage of shorter pellets.

### ACKNOWLEDGMENTS

Liguang Wang gratefully acknowledges financial support from The University of Queensland for his period of sabbatical leave at Cambridge. Grace Zhen Li Ng and Chia Wei Lim were University of Cambridge MEng students. The authors thank Harry Ayton for assistance with experiments.

### AUTHOR CONTRIBUTIONS

**Ligaung Wang:** Conceptualization; data curation; formal analysis; funding acquisition; investigation; methodology; validation; writing-original draft; writing-review and editing. **Chia Wei Lim:** Data curation; investigation; methodology; validation; writing-review and editing. **Grace Ng:** Data curation; investigation; methodology; validation; visualization; writing-review and editing. **Sarah Rough:** Conceptualization; formal analysis; methodology; project administration; supervision; writing-original draft; writing-review and editing. **Ian Wilson:** Conceptualization; data curation; formal analysis; project administration; resources; supervision; validation; writing-original draft; writing-review and editing.

## NOMENCLATURE

### Roman

| | |
|---|---|
| $D$ | extrudate diameter; extrusion die diameter (m) |
| $D_c$ | critical extrudate diameter, Equation (1) (m) |
| $D^*$ | scaled extrudate diameter |
| $F$ | force (N) |
| $H$ | protuberance height (m) |
| $k_N$ | overall pseudo rate constant, Equation (5) ($s^2$) |
| $k_{i,j}$ | pseudo rate constant, breakage model ($s^2$) |
| $L$ | die land length (m) |
| $n_i$ | number of $i$-unit pellets or species A, B |
| $N$, $N_0$ | total number of pellets, initial number |
| $N^*$ | normalized number of pellets, Equation (2) |
| $R$ | radius of spheronization plate (m) |
| $R^2$ | coefficient of determination |
| $S$ | protuberance base width (m) |
| $t$ | time (s) |
| $t_s$ | time to complete spheronization (s) |
| $u_i$ | rod velocity (m $s^{-1}$) |
| $v_{ram}$ | extruder ram velocity (m $s^{-1}$) |
| $w^*$ | dimensionless gap width, Equation (3) |
| $W$ | protuberance top width (m) |

### Greek

| | |
|---|---|
| $\omega$ | rotational speed of spheronization plate (rad $s^{-1}$) |
| $\beta$ | gain in pellet number, Equation (5) |
| $\theta$ | protuberance sharpness angle |
| $\rho$ | density (kg $m^{-3}$) |
| $\tau$ | scaled time, = $\omega^3 t$ ($s^{-2}$) |

## DATA AVAILABILITY STATEMENT

The data that support the findings of this study are available from the corresponding author upon reasonable request.

## ORCID

*D. Ian Wilson* https://orcid.org/0000-0003-3950-9165

## REFERENCES

1. Muley S, Nandgude T, Sushilkumar Poddar N. Extrusion–spheronization a promising pelletization technique: in-depth review. *Asian J Pharm Sci*. 2016;11:684-699.
2. Wilson DI, Rough SL. Extrusion-spheronisation. In: Salman AD, Hounslow MJ, Seville JPK, eds. *Granulation*. Amsterdam, Netherlands: Elsevier; 2006:189-210.
3. Bouffard J, Cabana A, Chaouki J, Bertrand F. Experimental investigation of the effect of particle cohesion on the flow dynamics in a spheronizer. *AIChE J*. 2012;59(5):1491-1501.
4. Koester M, Thommes M. Analysis of particle kinematics in spheronisation via particle image velocimetry. *Eur J Pharm Biopharm*. 2013;83:307-314.
5. Bryan MP, Atherton LN, Duffield S, Rough SL, Wilson DI. Stages in spheronisation: evolution of pellet size and shape during spheronisation of microcrystalline cellulose-based paste extrudates. *Powder Tech*. 2015;270:163-175.
6. Lau CLS, Yu Q, Lister VY, Rough SL, Wilson DI, Zhang M. The evolution of pellet size and shape during spheronisation of an extruded microcrystalline cellulose paste. *Chem Eng Res Des*. 2014;92(11):2413-2424.
7. Parkin J, Widjaja KS, Bryan MP, Rough SL, Wilson DI. Experimental validation of a dimensional analysis of spheronisation of cylindrical extrudates. *Powder Tech*. 2016;298:73-83.
8. Sinka IC. A first order numerical study of the spheronisation process. *Powder Tech*. 2011;206:195-200.
9. Sinka IC. A model for the deformation of an ellipsoid subject to a large number of successive impacts with special reference to spheronisation. *Powder Tech*. 2015;270:592-598.
10. Weis D, Evers M, Thommes M, Antonyuk S. DEM simulation of the mixing behavior in a spheronization process. *Chem Eng Sci*. 2018;192:803-815.
11. Zhang M, Li XK, Wilson DI, Yao TT, Zhang YY. Influence of the dimensions of spheroniser plate protuberances on the production of pellets by extrusion-spheronisation. *Adv Powder Tech*. 2018;29:1128-1141.
12. Liew CV, Chua SM, Heng PWS. Elucidation of spheroid formation with and without the extrusion step. *AAPS Pharm Sci Tech*. 2007;8:1-10.
13. Koester M, Willemsen E, Krueger C, Thommes M. Systematic evaluations regarding interparticular mass transfer in spheronisation. *Int J Pharm*. 2012;431(1–2):84-89.
14. Ramikrishna D, Singh MR. Population balance modeling: current status and future prospects. *Ann Rev Chem Biomol Eng*. 2014;5:123-146.
15. Zhang M, Li Y, Xing JF, Rough SL, Wilson DI. Influence of plate surface protuberance size and shape on the production of pellets by extrusion-spheronisation. *Chem Eng Res Des*. 2016;109:97-107.
16. Dorao CA, Jakobsen HA. A least squares method for the solution of population balance problems. *Comp Chem Eng*. 2006;30(3):535-547.
17. Zhang M, Rough SL, Ward R, Seiler C, Wilson DI. A comparison of ram extrusion by single-holed and multi-holed dies for extrusion-spheronisation of microcrystalline-based pastes. *Int J Pharm*. 2011;416:210-222.
18. Rough SL, Bridgwater J, Wilson DI. Effects of liquid phase migration on extrusion of microcrystalline cellulose pastes. *Int J Pharm*. 2000;204(1–2):117-126.
19. Bryan MP, Rickenbach J. MEng project report. Department of Chemical Engineering and Biotechnology, University of Cambridge; 2012.
20. Zhang M, Li Y. Spheronisation of a basket screen-extruded paste using screens of different hole diameters. *Powder Tech*. 2016;299:199-209.
21. Kumar R, Ketterhagen W, Sarkar A, Curtis J, Wassgren C. Breakage modeling of needle-shaped particles using the discrete element method. *Chem Eng Sci X*. 2019;3:100027.
22. Beeckman JWL, Fassbender NA, Datz TE. Length to diameter ratio of extrudates in catalyst technology II. Bending strength versus impulsive forces. *AIChE J*. 2016;62(8):2658-2669.
23. Delaney GW, Morrison RD, Sinnotta MD, Cummins S, Cleary PW. DEM modelling of non-spherical particle breakage and flow in an industrial scale cone crusher. *Miner Eng*. 2015;74:112-122.

## SUPPORTING INFORMATION

Additional supporting information may be found online in the Supporting Information section at the end of this article.

**How to cite this article:** Wang L, Lim CW, Ng GZL, Rough SL, Ian Wilson D. Modeling the breakage stage in spheronization of cylindrical paste extrudates. *AIChE J*. 2021;67:e17247. https://doi.org/10.1002/aic.17247